

## Article

# Mineralogical Evidence for Hydrothermal Uranium Mineralization: Discovery and Genesis of the Uranyl Carbonate Minerals in the BLS U Deposit, SW Songliao Basin, Northeast China

Bo Ding <sup>1,2</sup>, Hongxu Liu <sup>2</sup>, Deru Xu <sup>1,\*</sup>, Linfei Qiu <sup>1,2</sup> and Weihong Liu <sup>2</sup>

<sup>1</sup> State Key Laboratory Breeding of Nuclear Resource and Environment, East China University of Technology, Nanchang 330013, China

<sup>2</sup> CNNC Key Laboratory of Uranium Resource Exploration and Evaluation Technology, China Beijing Research Institute of Uranium Geology, Beijing 100029, China

\* Correspondence: xuderu@gig.ac.cn; Tel.: +86-0791-83897197

**Abstract:** Diabase intrusions have been widely found in sandstone-type U deposits of the south-western Songliao Basin, indicating diabase-related hydrothermal fluids might play an important role in this type of U mineralization. The first discovery of U-bearing carbonate minerals in the BLS U deposit provides an opportunity for understanding hydrothermal U mineralization and its relationship to diabase intrusions. U-bearing carbonate minerals occurred as thin shells generally ringing ankerite and then surrounded by colloidal pyrite through examination of scanning electron microscopy and energy dispersive spectroscopy. They can be interpreted as uranyl carbonate minerals, with the empirical formula of  $\text{Ca}_{2.7}\text{Fe}_{0.9}\text{Mg}_{0.4}(\text{UO}_2)(\text{CO}_3)_5 \cdot 9.6\text{H}_2\text{O}$ , based on infrared absorption spectroscopy and electron microprobe. The formation of uranyl carbonate minerals is most likely related to the  $\text{CO}_2$ -rich hydrothermal fluids from diabase intrusions according to its occurrence state, but the key factors are that the Ca-UO<sub>2</sub>-CO<sub>3</sub> ternary complexes should have been produced in ore-forming hydrothermal fluids and adsorption of ankerite on ternary complexes. Thereby, a potential diabase-related hydrothermal U mineralization model for sandstone-type U deposits can be proposed. The ore-forming fluids that originated from diabase-related hydrothermal are formed through continuously extracting the adsorbed U<sup>6+</sup> and dissolving the early U minerals. Then, U in the ore-forming hydrothermal fluids was migrated and transported probably either as uranyl carbonate ions or as Ca-UO<sub>2</sub>-CO<sub>3</sub> ternary complexes. The former is easy to precipitate in the form of pitchblende dispersed in the fossil wood cells, ringing pyrite, and occurring along the edge of adsorbents at the site of reducing capacity change, while the latter will extremely inhibit the reduction of U<sup>6+</sup>, eventually leading to the precipitation of uranyl carbonate minerals ringing ankerite by adsorption. The above research results can provide mineralogical evidence for hydrothermal U mineralization in sandstone-type U deposits of the Songliao Basin.

**Keywords:** hydrothermal U mineralization; uranyl carbonate minerals; Ca-UO<sub>2</sub>-CO<sub>3</sub> ternary complexes; sandstone-type U deposit; Songliao Basin



**Citation:** Ding, B.; Liu, H.; Xu, D.; Qiu, L.; Liu, W. Mineralogical Evidence for Hydrothermal Uranium Mineralization: Discovery and Genesis of the Uranyl Carbonate Minerals in the BLS U Deposit, SW Songliao Basin, Northeast China. *Minerals* **2023**, *13*, 339. <https://doi.org/10.3390/min13030339>

Academic Editor: Iuliu Bobos

Received: 22 November 2022

Revised: 22 December 2022

Accepted: 15 February 2023

Published: 28 February 2023



**Copyright:** © 2023 by the authors. Licensee MDPI, Basel, Switzerland. This article is an open access article distributed under the terms and conditions of the Creative Commons Attribution (CC BY) license (<https://creativecommons.org/licenses/by/4.0/>).

## 1. Introduction

In Northern China, the primary type of U (Uranium) deposits are the sandstone-type, which have been discovered in the Mesozoic sedimentary basins [1]. From west to east, U deposits are largely hosted in the Yili Basin (e.g., the Kujie’ertai, Zhajisitan, Mengqigu’er, and Wuku’erqi deposits) [2–4], the Ordos Basin (e.g., Zaohuohao, Nalinggou, and Daying deposits) [5–8], the Erlian Basin (e.g., the Nuheting, Saihangaobi, and Bayinwula deposits) [9–11], and the Songliao Basin (e.g., the Qianjadian and Baxingtu deposits) [12–14]. The mineralization mechanism of the sandstone-type U deposits has

been generally considered to be the oxidation-reduction interaction of epigenetic U-O-bearing fluids with reducing agents within permeable sandstones under low-temperature conditions, where soluble  $U^{6+}$  can be reduced to insoluble  $U^{4+}$  by detrital plant debris [15], hydrocarbons [16,17] and sulfides [18,19], and U minerals such as coffinite and pitchblende are mainly found in redox zone sandstone [20–23]. In recent years, increasing lines of evidence (e.g., hydrothermally altered minerals, fluids temperature, C-H-O-S isotope of altered minerals) have been accumulated to show that sandstone-type U deposits were subjected to the transformation of hydrothermal fluids with different sources, properties and driving forces, which is 5–10 °C higher than the maximum buried paleotemperature of the ore-bearing layer [24], such as the Azelik deposit in Niger [25], Savabuqi deposit in Tarim Basin [26]; Dongsheng deposit in Ordos Basin [27,28], Tamusu deposit in Bayongobi Basin [29,30], Qianjiadian deposit in Songliao Basin [12,13,31–37]. However, there was still no direct evidence for hydrothermal U mineralization, such as hydrothermal U minerals or U minerals related to hydrothermal activities, so it is still unclear whether hydrothermal fluids participate in U mineralization and in what way.

The latest research shows that diabase intrusions closely related to U mineralization in time and space have been widely found in sandstone-type U deposits of the southwestern Songliao Basin, indicating diabase intrusions and associated hydrothermal fluids maybe play an obvious role in sandstone-type U mineralization [12,13,31–37]. This is probably supported by well-developed hydrothermal alteration of ferrodolomitization, pyritization, hydromicazation and sericitization [12,13,31–34], and the change in mineralization environment with hydrothermal fluid activity, which can result in activation of the early U orebody and superimposed enrichment mineralization [12,13]. As a result, it provides an opportunity for innovation in the traditional low-temperature metallogenic theory of sandstone-type U deposits, which will contribute to guiding the prospecting and exploration of such types U deposits. The present paper focuses on U-bearing carbonate minerals first discovered in the BLS U deposit and aims to provide mineralogical evidence for hydrothermal U mineralization and insights into the mineralization-associated hydrothermal process(es). Consequently, SEM (scanning electron microscopy), EDS (energy dispersive spectroscopy), EPMA (electron microprobe), and infrared absorption spectroscopy were used to determine the mineralogical characteristics and genesis of U-bearing carbonate minerals and to reveal altered mineral assemblages containing U-bearing minerals of diabase-related hydrothermal origin.

## 2. Geological Setting

### 2.1. Songliao Basin

The Songliao Basin of northeast China is a large-scale continental sedimentary basin with multiple sedimentary cycles (Figure 1a). This basin, which is surrounded by the Great Xing'an Range to the west, the Lesser Xing'an Range to the north, and the Zhangguangcai Range to the east [38] (Figure 1a), can be subdivided into seven major tectonic units (Figure 1a), i.e., the Northern Plunge, the Central Depression, the North-east Uplift, the Southeast Uplift, the Western Slope, the Southwest Uplift and the Kailu Depression, from northeast to southwest. The basement of the Songliao Basin is mainly composed of Precambrian to Palaeozoic metamorphic rocks, Palaeozoic to Mesozoic granites, Palaeozoic sedimentary strata, and Late Jurassic intermediate to felsic volcanic rocks [14]. In turn, overlying the basement are the Mesozoic to Cenozoic clastic sediments of about 10 km thicknesses (Figure 1b), from lower to upper, including the Lower Cretaceous Shahezi, Yingcheng, and Denglouku formations, the Upper Cretaceous Quantou, Qingshankou, Yaojia, Nenjiang, Sifangtai, and Mingshui formations, the Paleogene Yi'an Formation, and the Neogene and Quaternary Da'an and Taikang formations [12]. Based on the previous works [39–41], the Songliao Basin suffered four main stages of tectonic evolution (Figure 1b): (i) a pre-rift stage of mantle upwelling represented by the Late Jurassic volcanic rocks of 157–147 Ma ages and the alluvial and shallow lacustrine sediments; (ii) a syn-rift stage characterized by the formation of fault-bounded basins and the deposition

of alluvial, fluvial and deep lacustrine sediments containing volcanoclastics in isolated rift grabens; (iii) a post-rift stage depicted by a switch from tectonic to thermal subsidence of a broad downward depression extended throughout the whole basin and the deposition of alluvial, fluvial and shallow to deep lacustrine sediments; and (iv) a structural inversion stage occurring since the end of the Late Cretaceous during deposition of the Sifangtai and Mingshui formations, characterized by the development of NNE-striking reverse faults, broad anticlines or domes [41,42].

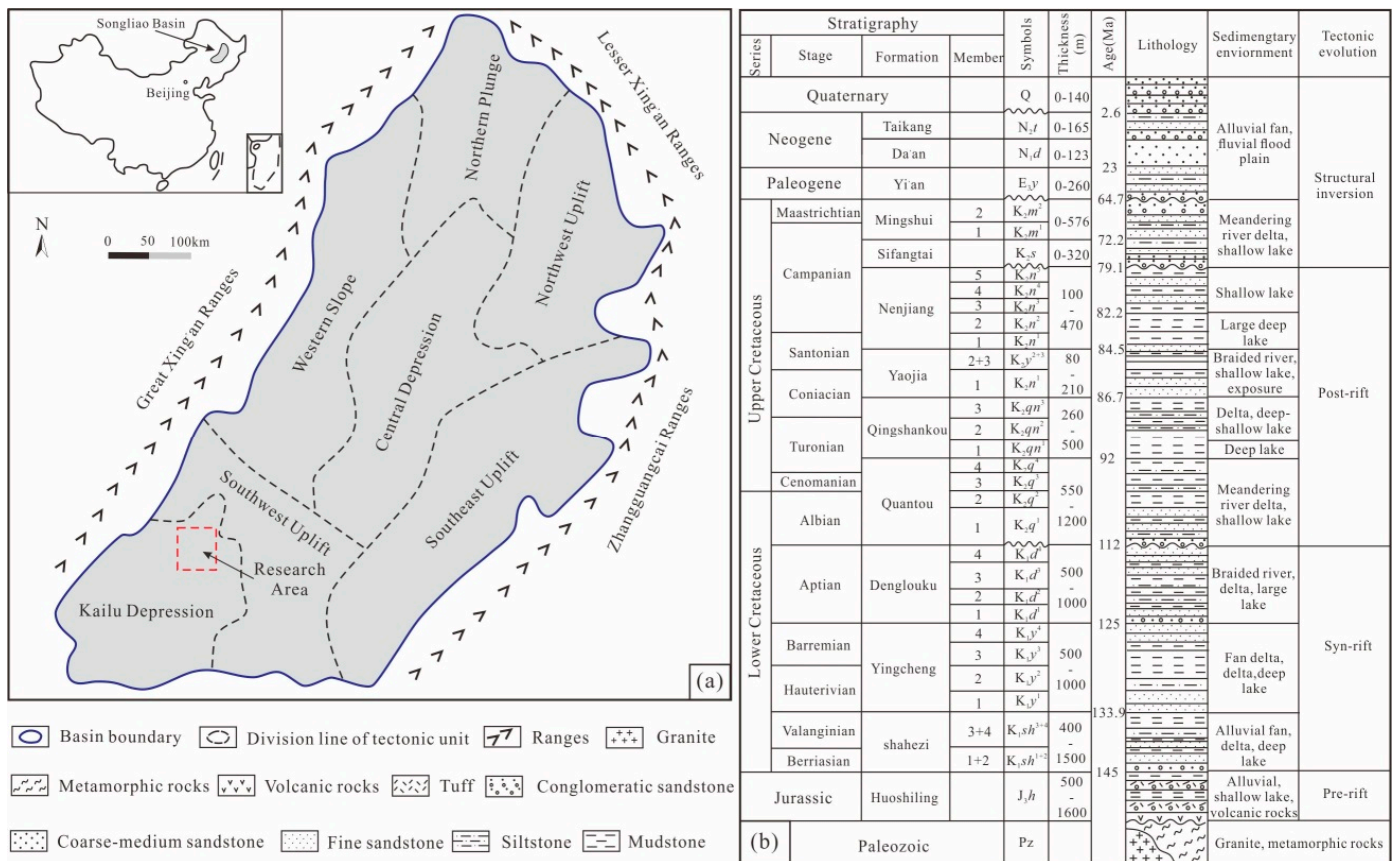
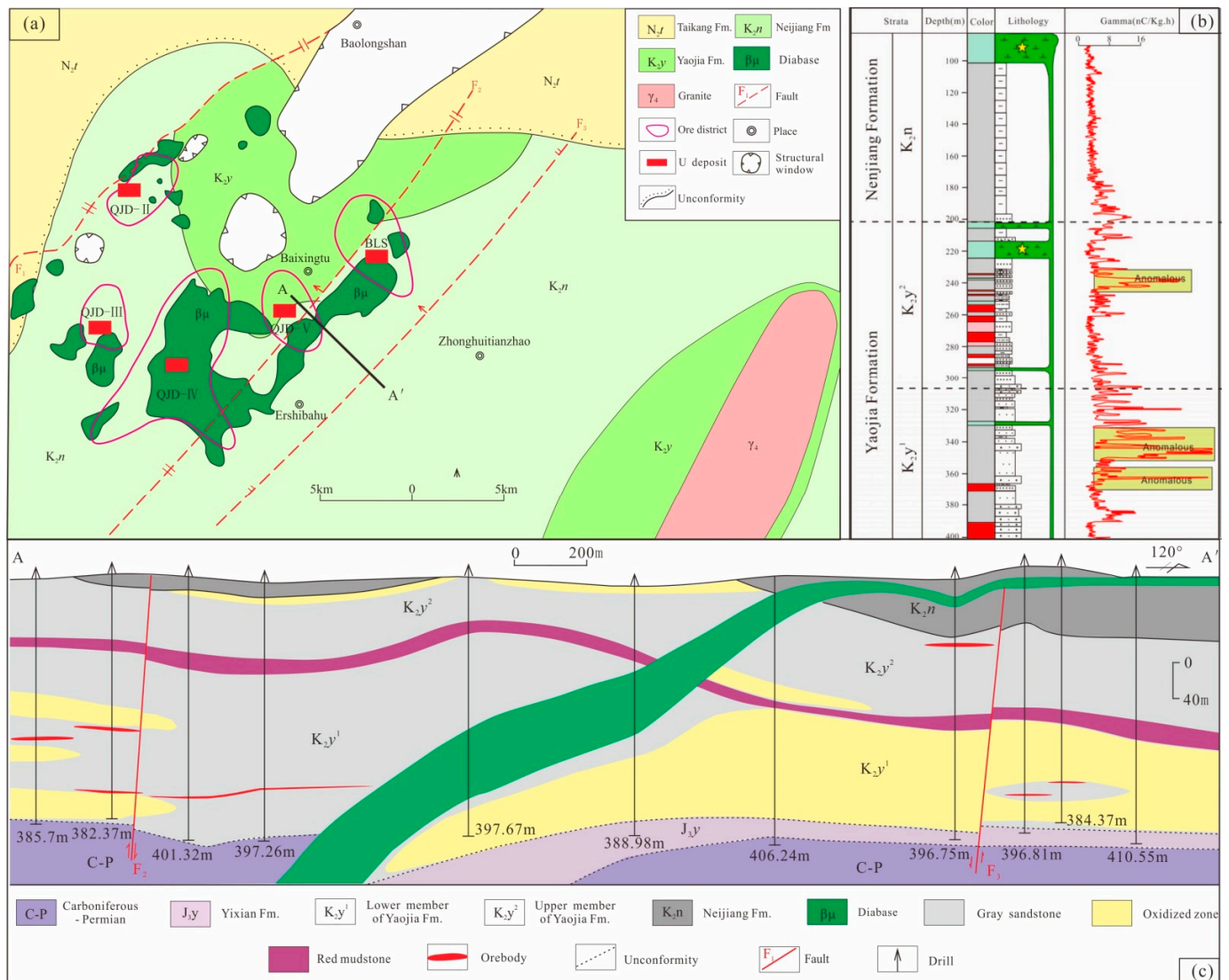


Figure 1. The tectonic units (a) and the stratigraphical framework and tectonic evolution (b) of the Songliao Basin, modified from [14].

2.2. The Baolongshan U Deposit

The northern part of the Qianjiadian Sag, a secondary tectonic unit of the Kailu depression, hosts abundant U mineralization, highlighted by the Qianjiadian (QJD-II, QJD-III, QJD-IV) and Baolongshan (BLS) U deposits (Figure 2a). These deposits are situated around the Baixingtu structural window formed by tectonic inversion at the end of the Late Cretaceous Nenjiang movement and are controlled by the faults (F1, F2, F3) that are revealed by fractured shatter zones and diabase dyke fillings [11–23,32,35–37] (Figure 2a). The BLS U deposit is located in the SE Baixingtu structural window and is controlled by faults F2 and F3 formed from the basin structural inversion (Figure 2a). It is hosted within the sandstone layers of the Lower member of the Yaojia Formation (Figure 2b). The Lower member has a 50–200 m thickness in an interval between 280 m and 400 m below the surface and accounts for the main depositional setting for braided river facies under arid and semi-arid conditions. Lithologically, this member comprises red and purplish-red mudstones (5–15 m) at the top (i.e., primary oxidation zone), light- and brown-yellow medium- to coarse-grained sandstones at the upper section (i.e., epigenetic oxidation zone), gray fine-medium-coarse-grained sandstones in the lower section (i.e., redox zone), and brownish yellow medium-coarse grained sandstones at the bottom (i.e., epigenetic oxidation zone).

U mineralization occurred at the redox zone, with sulfide, plant stems, or charcoal chips generally observed in the ore-bearing sandstones. Morphologically, U orebodies are tabular and/or lenticular, while to date, no roll-front style has been reported [12–14]. U minerals are mainly pitchblende, which is often produced around reducing substances such as pyrite and organic matter in colloidal form or adsorbed on the surface of clay minerals, mica, and debris particles in small particles [43,44]. Through U-Pb isotopic analysis of the bulk ores and single U minerals [43,44], previous studies have captured the mineralization ages of  $40 \pm 3$  Ma,  $53 \pm 3$  Ma,  $67 \pm 5$  Ma, and  $96 \pm 14$  Ma for the ore deposits in QJD-BLS, indicating multi-stage U mineralization.



**Figure 2.** Pre Quaternary geological map (a), columnar sections of U-bearing layer (b) of QJD-BLS mining area, (c) SW Songliao Basin, modified from [13].

Diabase dikes, which generally have an orientation to NE (Figure 2a) and cut through the Lower and Upper Yaojia members of the Late Cretaceous Yaojia Formation and the Neijiang Formation (Figure 2c), are well developed and mainly controlled also by faults F2 and F3 in the mining district (Figure 2a). Furthermore, previous works proposed that the emplacement ages of the diabase dikes are  $45.8 \pm 8$  Ma,  $49.4 \pm 5$  Ma,  $51.7 \pm 0.3$  Ma, and  $53 \pm 2.3$  Ma using the Ar-Ar dating method [37], and  $47 \pm 1$  Ma,  $42 \pm 1$  Ma,  $40 \pm 1$  Ma using zircon U-Pb dating method [35]. Therefore, the primary mineralization ages of 53 Ma to 28 Ma [13,43,44] for the regionally interstratified oxidized U deposits are consistent

with the emplacement timings for the swarms of diabase dikes. This indicates that diabase emplacement and associated hydrothermal fluids might play an important role in sandstone-type U mineralization [12,13,31–37]. The temperature measurement results of inclusions in calcite veins of calcareous sandstones show that the early hydrothermal fluids related to diabase intrusions have higher temperatures (203–234 °C) and lower salinity [13]. With the interaction with the ore-bearing sandstones, the temperature of the hydrothermal fluids decreases and the salinity increases, and a series of carbonate cements were generated as calcite and ankerite, which is consistent with the temperature (100–232 °C) measurement results of inclusions in carbonate cement of calcareous sandstone [12,13]. In addition, the composition measurement results of fluid inclusions in carbonate cements indicate that the hydrothermal fluids associated with diabase intrusion have a local extremely high fugacity of CO<sub>2</sub> [13]. Moreover, colloidal pyrite of TSR origin was also formed in the above process of fluid-rock interaction [13]. Therefore, we believe that the formation of ankerite and colloidal pyrite is related to hydrothermal fluids related to diabase intrusions.

### 3. Sampling and Analytical Methods

In this study, the ore-bearing sandstone samples (n = 15) located near diabase intrusions or obviously transformed by hydrothermal fluids were collected from several boreholes in the BLS mining district with the purpose of providing mineralogical evidence for hydrothermal U mineralization. Initially, carbon-coated blocks (n = 10) and polished sections (n = 15) of the sandstone samples were examined with scanning electron microscopy and energy dispersive spectroscopy in order to find out the occurrence state of U and looking for U minerals related to hydrothermal fluids. Then, an electron microprobe was carried out for possible hydrothermal U minerals to determine their chemical composition and occurrence state. Finally, infrared absorption spectroscopy was used to identify the mineral types of possible hydrothermal U minerals. The above works were carried out at the Analysis and Test Center of Beijing Research Institute of U Geology.

The high-resolution field emission scanning electron microscope of ZEISS sigma300 (Carl Zeiss Microscopy Deutschland GmbH, Oberkochen, Germany) has an acceleration voltage of 20 kV, a working distance of 10 mm, and secondary electron (SE) imaging resolution under low vacuum, 1.5 nm, 30 kV and under high vacuum, 1.0 nm, and 15 kV. The backscattering condition of 30 kV is better than that of 1.5 nm, while the backscattering condition of 10 kV is better than that of 3.5 nm. The magnification ranges from 20–1,000,000 times. The OXFORD X-MAX80 model of the spectrometer has the pulse processor set at 275 kcps, the input counting rate between 300 and 450 cps, and the analytical elements of Be-U.

The JXA-8100 model of the electron microprobe was used in this study. The acceleration voltage and beam current were 20 kV and 10 nA, respectively. The beam spot diameter was 2–5 μm, and counting times were 10–15 s. The quantitative spectral analysis and calibration method was used with the SPI 53 minerals standard (U.S.) and the PRZ correction, respectively. Therein, the CO<sub>2</sub> and H<sub>2</sub>O content are equivalently calculated according to the total number of cations.

Mid-infrared spectra were obtained using the BRUKER LUMOS Micro-FTIR within an ATR model. The spectra were obtained after 64 scans with a scanning range between 4000 and 640 cm<sup>-1</sup> and a resolution of 4 cm<sup>-1</sup>. Data processing and spectral manipulation, such as smoothing, baseline adjustment, normalization, and band component analysis, were performed using the special software OPTU 7.5 as an accessory instrument.

## 4. Results

### 4.1. U Minerals and Their Occurrences

The samples in the present study are all gray and gray-white ore-bearing sandstones (U content > 300 ug/g), rich in organic matter and pyrite, and generally characterized by high calcium content (Figure 3a–c). Analysis from SEM and BSE images indicates that the U minerals in the studied deposits are mainly pitchblende (Figure 3), with a small amount of U-bearing TiO<sub>2</sub> (Figure 3d). Pitchblende mainly presents in intergranular pores and coexists

with pyrite, fossil wood cells, kaolinite, and other adsorbents. Some pitchblende grains are dispersed in the fossil wood cells (Figure 3j) or grown surrounding pyrite (Figure 3i), whereas those tiny pitchblende grains often appear as star dots or aggregates within the interstitial materials of intergranular pores (Figure 3d,e), along the edges of kaolinite (Figure 3f), and/or in dissolution pores of potash feldspar (Figure 3e). The most significant is that U-bearing carbonate minerals are discovered in ore-bearing sandstones and occurred as thin shell ringing ankerite through an examination on SEM and EDS (Figures 3k,i and 4). In addition, the unique and important geological phenomenon that U-bearing ankerite can be seen in some samples around ankerite and then surrounded by colloidal pyrite (Figure 4c,d) indicates that U-bearing carbonate minerals were formed after ankerite and before colloidal pyrite.

#### 4.2. Chemical Composition of the U-Bearing Carbonate Minerals

The infrared-absorption spectrum of the U-bearing carbonate minerals from the studied deposits in the Songliao Basin is shown in Figure 5a and commonly exhibits similar assignments of absorption bands to that of the Oswaldpeetersite  $(\text{UO}_2)_2\text{CO}_3(\text{OH})_2 \cdot 4\text{H}_2\text{O}$  from Renaud (Figure 5b) [45], Swartzite  $(\text{CaMg}[\text{UO}_2(\text{CO}_3)_3] \cdot 12\text{H}_2\text{O})$  from Samer [46], revealing that the U-bearing carbonate minerals occupy  $\text{CO}_3^{2-}$ , (O-U-O) and (H-O-H) chemical compositions, extremely consistent with the EMPA analysis (Table 1). As shown in Table 2, band at  $\sim 1636 \text{ cm}^{-1}$  is assigned to vibration of H-O-H bending,  $\sim 907 \text{ cm}^{-1}$  and  $\sim 881 \text{ cm}^{-1}$  are assigned to vibration of O-U-O antisymmetric stretching,  $\sim 1522 \text{ cm}^{-1}$ ,  $\sim 1403 \text{ cm}^{-1}$ ,  $\sim 1127 \text{ cm}^{-1}$ ,  $\sim 1000 \text{ cm}^{-1}$ ,  $\sim 779 \text{ cm}^{-1}$  and  $698 \text{ cm}^{-1}$  are assigned to vibration of the  $\text{CO}_3^{2-}$  anions. As shown in Table 2,  $\text{UO}_2$  content ranges from 25.60% to 28.80%, with an average of 27.43%, CaO from 15.08% to 15.35%, with an average of 15.33%, FeO from 6.44% to 7.22%, with an average of 6.70% and MgO from 1.34% to 1.65%, with an average of 1.48%. Nevertheless, the  $\text{H}_2\text{O}$  and  $\text{CO}_2$  concentrations are not determined directly by EMPA analysis, resulting in relatively low total contents. In addition, the U-bearing carbonate minerals also contain many impurities through EMPA analysis, which most likely were caused by the absorption of clay minerals on the surface.

**Table 1.** Analyses result of an infrared-absorption spectrum of U-bearing carbonate minerals.

Wavenumber ( $\text{cm}^{-1}$ ) of Oswaldpeetersite from Renaud [45]	Vibrational Mode	Wavenumber ( $\text{cm}^{-1}$ ) of U-Bearing Carbonate Minerals from This Study
1636	$\delta$ (H-O-H) bending	1635
1520, 1374	$\nu_3$ ( $\text{CO}_3^{2-}$ ) antisymmetric stretching	1522, 1403
1114	$\nu_1$ ( $\text{CO}_3^{2-}$ ) symmetric stretching	1127, 1000
915	$\nu_3$ (O-U-O) antisymmetric stretching	907, 881
804	$\nu_2$ ( $\text{CO}_3^{2-}$ ) out-of-plane bending	779
724	$\nu_4$ ( $\text{CO}_3^{2-}$ ) in-plane bending	698

**Table 2.** Average chemical compositions of U-bearing carbonate minerals by EPMA.

Test Point	FeO (%)	$\text{UO}_2$ (%)	MgO (%)	CaO (%)	Test Total (%)	$\text{CO}_3^{2-}$ (%)	$\text{H}_2\text{O}$ (%)
1	6.46	28.8	1.48	15.08	51.82		
2	7.22	25.6	1.46	15.18	49.46		
3	6.44	28.02	1.65	15.35	51.46		
4	6.66	27.3	1.34	15.71	51.01		
average	6.70	27.43	1.48	15.33	50.90	30.48	17.53

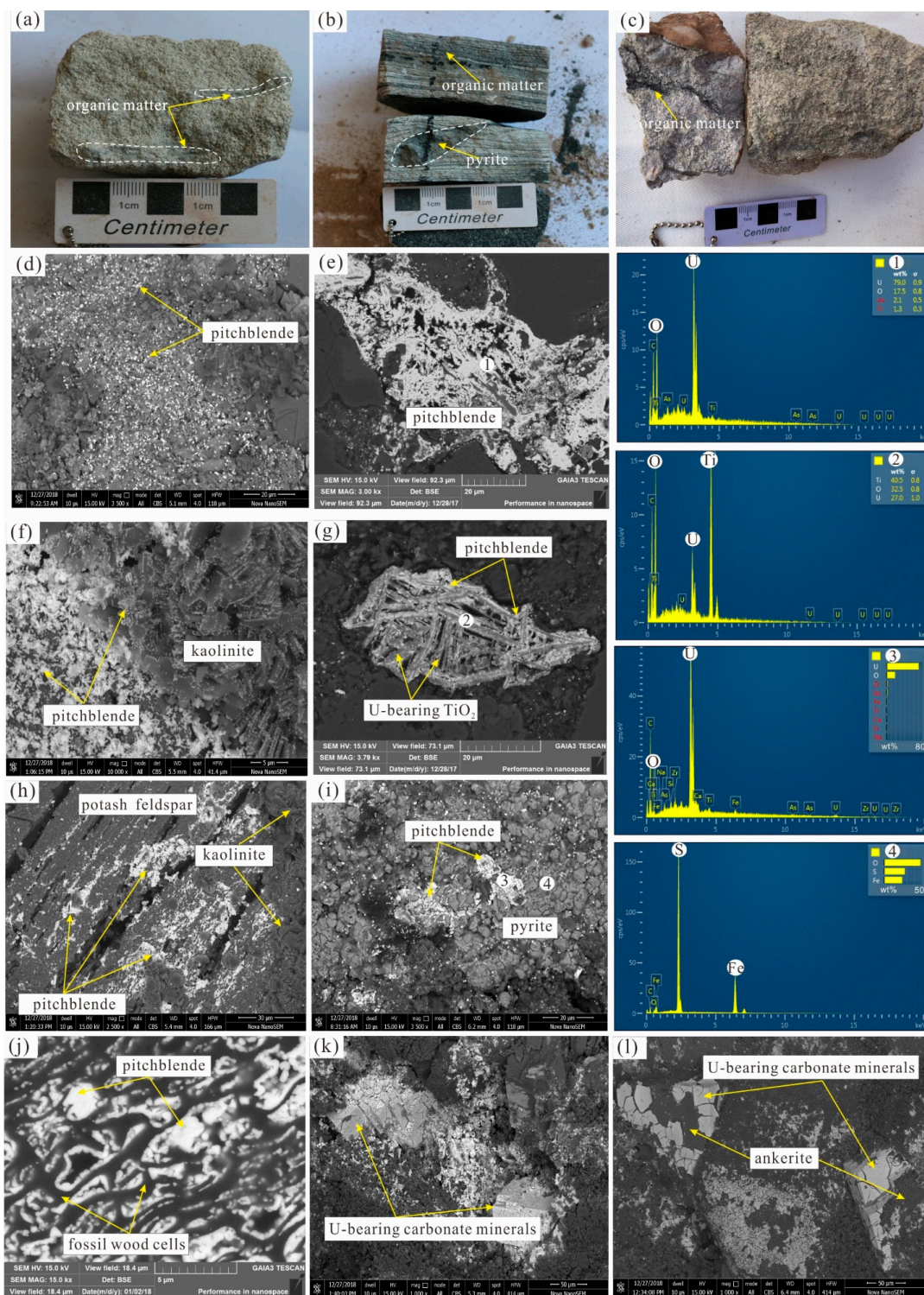


**Figure 3.** Back scattered electron (BSE) images showing the U occurrence in ore-bearing sandstone of BLS U deposit. (a) Gray-white calcareous ore-bearing medium sandstone, containing a small amount of organic matter; (b) Gray calcareous ore-bearing fine sandstone, containing pyrite and organic matter; (c) Gray calcareous ore-bearing gravelly coarse sandstone, containing organic matter; (d) Fine pitchblende adsorbed on fine sediments between particles; (e) Pitchblende aggregates occurring in intergranular pores; (f) Fine pitchblende adsorbed on kaolinite; (g) U-bearing  $TiO_2$ ; (h) Fine pitchblende adsorbed in pores of potash feldspar and on kaolinite; (i) Pitchblende aggregates around pyrite in intergranular pores; (j) Fine pitchblende in fossil wood cells; (k) U-bearing carbonate minerals in intergranular pores; (l) U-bearing carbonate minerals around ankerite in intergranular pores.

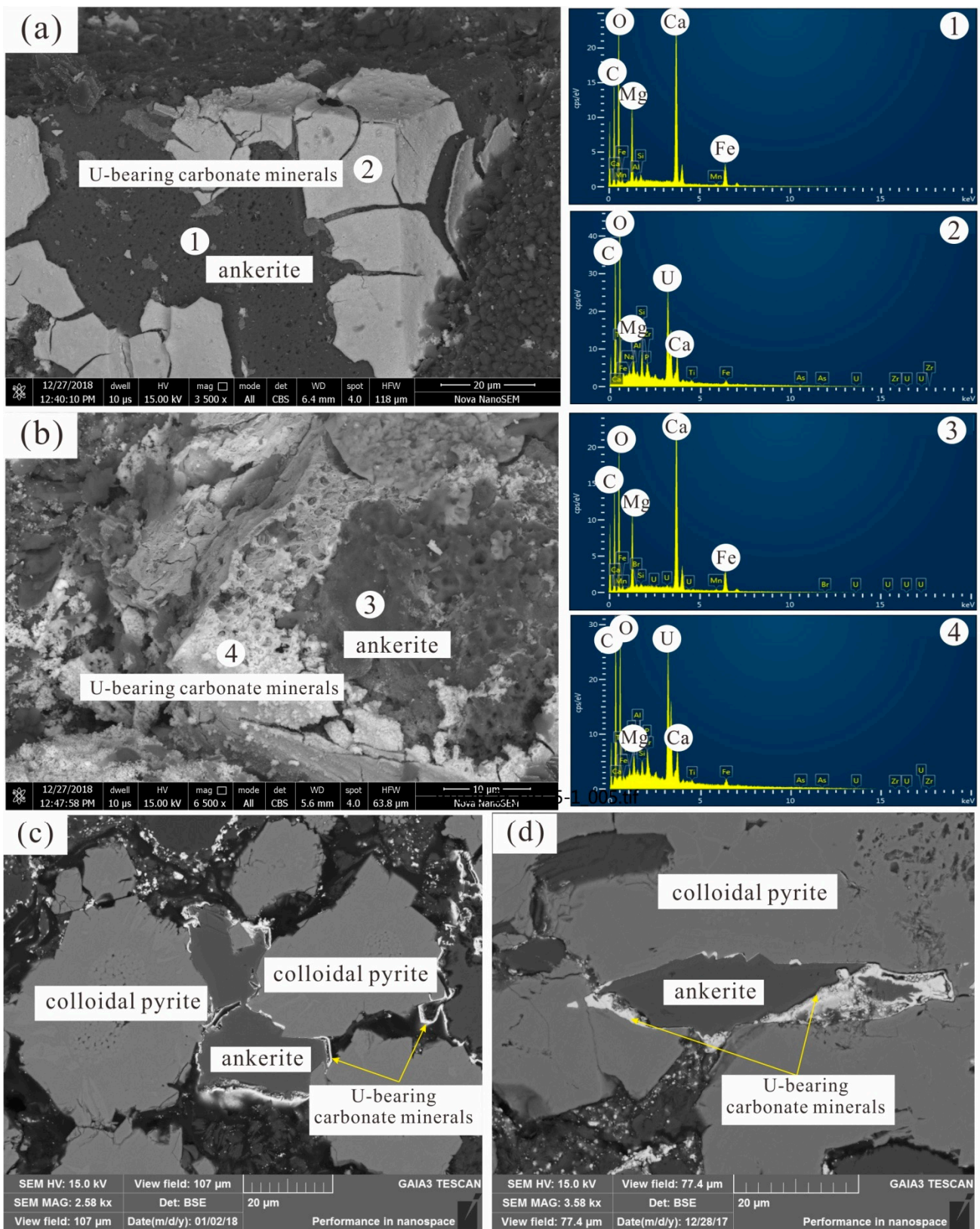


**Figure 4.** Back scattered electron (BSE) images showing the morphological characteristics of U-bearing ankerite. (a) U-bearing carbonate minerals occurred as a thin shell around the ankerite in intergranular pores; (b) U-bearing carbonate minerals occurred as a thin shell around the ankerite in intergranular pores; (c) U-bearing carbonate minerals around the ankerite and colloidal pyrite; (d) U-bearing carbonate minerals around ankerite, and then surrounded by colloidal pyrite.

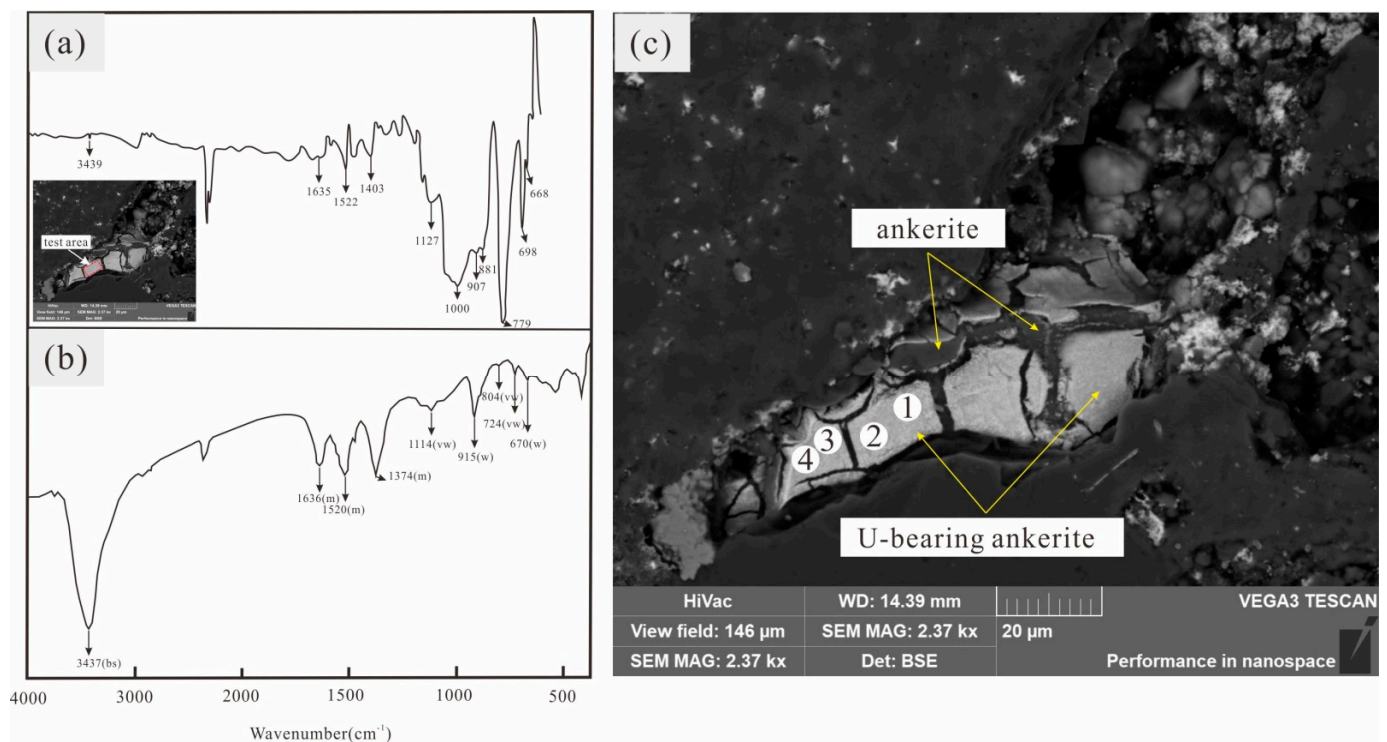


**Figure 5.** Analyses result of an infrared-absorption spectrum of U-bearing carbonate minerals (a) and Oswaldpeetersite (b) and EPMA (c) of U-bearing carbonate minerals.

## 5. Discussion

### 5.1. Mineral Types of Uranyl Carbonate Minerals

The results of the infrared absorption spectrum show that there are  $\text{CO}_3^{2-}$ , (O-U-O), and (H-O-H) in U-bearing carbonate minerals. Combined with the qualitative analysis of the energy spectrum, U-bearing carbonate minerals contain  $\text{Ca}^{2+}$ ,  $\text{Fe}^{2+}$ , and  $\text{Mg}^{2+}$  and thus are considered to be uranyl carbonate minerals. The chemical composition of the uranyl carbonate minerals shows that the average value of  $\text{UO}_2$  content is 27.43%,  $\text{CaO}$  content is 15.33%,  $\text{FeO}$  content is 6.70%,  $\text{MgO}$  content is 1.48%, and total content is 50.90%. It indicates that the average value of  $\text{CO}_3^{2-}$  and  $\text{H}_2\text{O}$  content accounts for 41.0%. Therefore, the empirical formula is  $\text{Ca}_{2.7}\text{Fe}_{0.9}\text{Mg}_{0.4}(\text{UO}_2)(\text{CO}_3)_5 \cdot 9.6\text{H}_2\text{O}$  through the calculation of chemical composition.

### 5.2. Genesis of Uranyl Carbonate Minerals

Uranyl carbonate minerals are typical secondary U minerals and generally occur under oxidizing and weak alkaline to alkaline conditions in the supergene zone as an oxidation zone and tunnel wall or waste rock heap of U deposits. However, the uranyl carbonate minerals in the BLS U deposit are all produced in gray and gray-white ore-bearing sandstones, rich in pyrite, organic matter, and other reducing substances visible (Figure 3a–c), and no iron oxide was found, indicating that the sandstones have not been modified by oxidation fluids. How were the uranyl carbonate minerals formed in the gray ore-bearing sandstones under a relatively reduced environment?

As shown in Figure 4, uranyl carbonate minerals, ankerite, and colloidal pyrite often coexist in the ore-bearing sandstones, suggesting that they may be formed at the same time. Moreover, uranyl carbonate minerals can be seen around ankerite and surrounded by colloidal pyrite (Figure 4c,d), indicating that uranyl carbonate minerals were formed after ankerite and before pyrite. A lot of previous studies have shown that the formation of ankerite and colloidal pyrite is related to the hydrothermal fluids associated with diabase intrusions [12,13,32,33]. Therefore, it is believed that the genesis of the uranyl carbonate minerals can also be linked to the wide emplacement of diabase dikes in the mining dis-

tract. In addition, previous workers suggested that the hydrothermal fluids associated with diabase emplacement were rich in cations such as  $\text{Ca}^{2+}$ ,  $\text{Fe}^{2+}$ , and  $\text{Mg}^{2+}$  and anions such as  $\text{HCO}_3^-$  and  $\text{CO}_3^{2-}$  [12,13]. The Ca–UO<sub>2</sub>–CO<sub>3</sub> ternary complexes (e.g.,  $\text{Ca}(\text{Fe}, \text{Mg})\text{UO}_2(\text{CO}_3)_3^{2-}$  and  $\text{Ca}(\text{Fe}, \text{Mg})_2\text{UO}_2(\text{CO}_3)_3$ ) could be formed in the hydrothermal fluids at a pH ranging from 7.5 to 9.0 and mM concentrations of  $\text{Ca}^{2+}$  ( $\text{Fe}^{2+}$ ,  $\text{Mg}^{2+}$ ) ions [47–49]. Once the Ca–UO<sub>2</sub>–CO<sub>3</sub> ternary complexes are formed, they need a lower redox potential of the medium environment to be reduced and inhibit the reduction of  $\text{U}^{6+}$  for the reductive substances [50,51]. Moreover, they are easy to be adsorbed on the surfaces of carbonate minerals to form uranyl carbonate minerals which are precipitated around them by molecular dynamics (MD) simulations [52]. Experiments for the precipitation of uranyl minerals on the surface of carbonate minerals also confirm this process [53,54]. As a result, the formation of ternary complexes and the adsorption of ankerite are the reasons for the formation of uranyl carbonate minerals in a reduction environment of the BLS U deposit. Uranyl carbonate minerals, discovered for the first time, and its associated minerals were considered to be related to the hydrothermal fluids caused by diabase intrusions, which provides mineralogical evidence for hydrothermal U mineralization in sandstone-type U deposits of the Songliao Basin.

### 5.3. Hydrothermal U Mineralization in Sandstone-Type U Deposits

The emplacement of the diabase intrusions in the QJD-BLS U mining district overlapped with the broad U mineralization (Figure 2a). Several boreholes revealed diabase intrusions in the form of dikes and walls in the Yaojia Formation, which finally intruded into the Nenjiang Formation and produced the form of layers and caps (Figure 2b,c). Moreover, the primary mineralization ages [13,43,44] for the regionally interstratified oxidized U deposits are consistent with the emplacement timings for the swarms of diabase dikes [35–37]. These lines of evidence indicate that spatiotemporally the sandstone-type U mineralization is closely related to diabase intrusions, and associated hydrothermal fluids might have played an important role in the formation of the sandstone-type U deposits [12,13,31–37]. However, there is still no direct evidence, such as U minerals of hydrothermal origin, to confirm the internal correlation between diabase emplacement and sandstone-type U mineralization. The discovery and genetic study of the uranyl carbonate minerals in this paper may provide a good bridge and opportunity for revealing the hydrothermal U mineralization model for sandstone-type U deposits of the Songliao Basin.

An increasing number of experimental studies have shown that U migration or precipitation depends not only on redox conditions but also on the physical and chemical characteristics of the fluids, such as chemical composition, pH, and temperature. For example, the formation of the stable Ca–UO<sub>2</sub>–CO<sub>3</sub> ternary complex requires a lower reducibility capacity for U reduction, which can significantly inhibit U reduction [50,51]. The increase in pH will increase the concentration of  $\text{HCO}_3^-$  and  $\text{CO}_3^{2-}$  ions in the fluid, which dramatically improves the fluid extraction and oxidation of U minerals [50,51,55]. The increase in temperature also increases the stability constant of uranyl complexes, indicating that they are more difficult to be reduced at high temperatures [27,56]. The research shows that the diabase intrusions can release a large amount of CO<sub>2</sub> gas [31,35], which can migrate to the ore-bearing layer along the faults and other favorable channels. It is easily dissolved in the formation water to form an acidic environment and interact with rock debris and feldspar in sandstones to form kaolinite [3–5], which are conducive to the adsorption in sandstone-type U deposits [18,57], resulting in a large number of tiny pitchblende present on the surface of clay minerals, TiO<sub>2</sub>, fine sediments between particles and other adsorbents (Figure 3). The above process is accompanied by the release of  $\text{K}^+$ ,  $\text{Ca}^{2+}$ ,  $\text{Fe}^{2+}$ ,  $\text{Mg}^{2+}$ , and other alkaline ions into the late CO<sub>2</sub>-rich hydrothermal fluids [3–5]. Carbonate minerals such as calcite, ankerite, and siderite precipitated successively due to changes in their internal CO<sub>2</sub> fugacity, temperature, and concentration of cations such as  $\text{Ca}^{2+}$ ,  $\text{Fe}^{2+}$ , and  $\text{Mg}^{2+}$  [12,13]. In addition, the ore-forming hydrothermal fluids are formed by continuously extracting the adsorbed  $\text{U}^{6+}$  in the ore-bearing sandstones and dissolving the U minerals

formed in the early stage under alkaline [50,51,55] and high-temperature conditions [27,56]. U in hydrothermal fluids can migrate in the form of uranyl carbonate ions or Ca-UO<sub>2</sub>-CO<sub>3</sub> ternary complexes [47–49]. The former complexes are easy to be reduced to U<sup>4+</sup> at the site of reducing capacity change and formed pitchblende dispersed in the fossil wood cells, around pyrite, and also adsorbed along the edge of adsorbents (e.g., kaolinite), consistent with the traditional sandstone-type U deposit [4,7]. The reduction of the latter complex requires a lower redox potential [50,51]. That is, the formation of the Ca-UO<sub>2</sub>-CO<sub>3</sub> ternary complexes will inhibit the reduction of U<sup>6+</sup> and then uranyl carbonate minerals will precipitate and occur as thin shells ringing the ankerite by adsorption. Finally, colloidal pyrite of TSR origin was formed in the process of interaction between hydrothermal fluids and sandstones, resulting in the occurrence of colloidal pyrite around ankerite and uranyl carbonate minerals. The above research results provide a hydrothermal U mineralization model for sandstone-type U deposits of the Songliao Basin.

## 6. Conclusions

(1) U minerals in the sandstone-type U deposits of the SW Songliao Basin are mainly pitchblende and occur in intergranular pores, and coexist with pyrite, fossil wood cells, kaolinite, and other adsorbents. U-bearing carbonate minerals, generally presented as thin shell ringing ankerite, are first discovered in the ore-bearing sandstones and can be interpreted as uranyl carbonate minerals with the empirical formula of Ca<sub>2.7</sub>Fe<sub>0.9</sub>Mg<sub>0.4</sub>(UO<sub>2</sub>)(CO<sub>3</sub>)<sub>5</sub>•9.6H<sub>2</sub>O.

(2) Uranyl carbonate minerals were considered to be related to the CO<sub>2</sub>-rich hydrothermal fluids from diabase intrusions according to their occurrence state, and thus provided direct mineralogical evidence for hydrothermal U mineralization. However, the preconditions for the generation of uranyl carbonate minerals are that there are Ca-UO<sub>2</sub>-CO<sub>3</sub> ternary complexes in ore-forming hydrothermal fluids and adsorption of ankerite on ternary complexes.

(3) The ore-forming hydrothermal fluids were formed by continuously extracting the adsorbed U<sup>6+</sup> and dissolving the early U minerals, and U migrates in the form of uranyl carbonate ions or Ca-UO<sub>2</sub>-CO<sub>3</sub> ternary complexes. The former is easy to precipitate in the form of pitchblende at the site of reducing capacity change, and the latter will extremely inhibit the reduction of U<sup>6+</sup>, eventually leading to the precipitation of uranyl carbonate minerals ringing ankerite. It provides a hydrothermal U mineralization model for sandstone-type U deposits of the Songliao Basin.

**Author Contributions:** Conceptualization, B.D. and H.L.; Sample, B.D. and L.Q.; methodology, B.D., L.Q. and W.L.; software, B.D., H.L. and W.L.; formal analysis, B.D.; investigation, B.D., L.Q. and H.L.; writing—original draft preparation, B.D., H.L. and D.X.; writing—review and editing, B.D., H.L., W.L. and D.X.; supervision, B.D., H.L. and D.X.; All authors have read and agreed to the published version of the manuscript.

**Funding:** This study was financially supported by the Fourth Talent Project from China National Nuclear Corporation (No. QNYC2103), Multi Coupling Geological Mineralization and Time-space Positioning Project of Sandstone-type U Deposit (No. (2021)143), and Project of China Nuclear Industry Geological Bureau (No. D2202, D2204, D2219).

**Data Availability Statement:** Not applicable.

**Acknowledgments:** We are highly thankful to Geologic Party No.243, China National Nuclear Corporation, for the permission to examine cores and field work investigation in the study areas. Our thanks are also given to the editors and reviewers for constructive comments that helped improve the paper.

**Conflicts of Interest:** The authors declare no conflict of interest.

## References

1. Hou, B.H.; Keeling, J.; Li, Z.Y. Paleovalley-related U deposits in Australia and China: A review of geological and exploration models and methods. *Ore Geol. Rev.* **2017**, *88*, 201–234. [[CrossRef](#)]

2. Zhang, C.; Liu, H.X. A growing sandstone type U district in South Yili Basin, NW China as a result of extension of Tianshan Orogen: Evidences from geochronology and hydrology. *Gondwana Res.* **2019**, *76*, 146–172. [[CrossRef](#)]
3. Ding, B.; Liu, H.X.; Li, P.; Jiang, H.; Zhang, H.J.; Zhang, B. The genetic mechanism of kaolinite in ore-bearing sandstone in the Mengqiguer U Deposit, Yili, and its relation with U mineralization. *Acta Geol. Sin.* **2019**, *93*, 2021–2036, (In Chinese with English Abstract).
4. Ding, B.; Liu, H.X.; Zhang, C.; Liu, H.; Li, P.; Zhang, B. Mineralogy, Fluid Inclusion and H-O-C-S Stable Isotopes of Mengqiguer U Deposit in the Southern Yili Basin, Xinjiang: Implication for Ore Formation. *Acta Geol. Sin. (Engl. Ed.)* **2020**, *94*, 1488–1503. [[CrossRef](#)]
5. Ding, B.; Liu, H.X.; Zhang, B. The formation mechanism of tabular orebody of sandstone—Type U in northern Ordos basin: Constraints on the study of kaolinite content from different zones of ore—Bearing sandstone. *Acta Geol. Sin.* **2020**, *94*, 2874–2882, (In Chinese with English Abstract).
6. Li, Z.Y.; Fang, X.H.; Chen, A.P.; Sun, Y.; Chen, F.; Liu, Z.; Zhang, K.; Zhou, W.; Li, M.; Jiao, Y. Superposition metallogenic model of sandstone-type U deposit in the Northeastern Ordos basin. *Uranium Geol.* **2009**, *25*, 65–70, (In Chinese with English Abstract).
7. Yi, C.; Wang, G.; Li, X.D.; Zhang, K.; Wang, Y.J. A tentative discussion on U enrichment characteristics and metallogenic model in Zhiluo Formation, northeastern Ordos Basin. *Miner. Depos.* **2018**, *37*, 835–852. (In Chinese with English Abstract)
8. Zhang, C.; Yi, C.; Dong, Q.; Cai, Y.Q.; Liu, H.X. Geological and geochronological evidence for the effect of Paleogene and Miocene uplift of the Northern Ordos Basin on the formation of the Dongsheng U district, China. *J. Geodyn.* **2018**, *114*, 1–18. [[CrossRef](#)]
9. Bonnetti, C.; Cuney, M.; Malartre, F.; Michels, R.; Li, X.; Peng, Y. The Nuheting deposit, Erlian Basin, NE China: Syndimentary to diagenetic U mineralization. *Ore Geol. Rev.* **2015**, *69*, 118–139. [[CrossRef](#)]
10. Bonnetti, C.; Cuney, M.; Michels, R.; Truche, L.; Malartre, F.; Liu, X.; Yang, J. The multiple roles of sulfate-reducing bacteria and Fe-Ti oxides in the genesis of the Bayinwula roll front-type U deposit, Erlian Basin, NE China. *Econ. Geol.* **2015**, *110*, 1059–1081. [[CrossRef](#)]
11. Nie, F.; Yan, Z.; Feng, Z.; Li, M.; Xia, F.; Zhang, C.; Wang, Y.; Yang, J.; Kang, S.; Shen, K. Genetic models and exploration implication of the paleo-channel sandstone-type U deposits in the Erlian Basin, North China—A review and comparative study. *Ore Geol. Rev.* **2020**, *127*, 103821. [[CrossRef](#)]
12. Nie, F.; Yan, Z.; Xia, F.; Li, M.; Feng, Z.; Lu, Y.; Cai, J. Mineralisation from hot fluid flows in the sandstone-type U deposit in the Kailu Basin, Northeast China. *Appl. Earth Sci.* **2018**, *127*, 2–14, (In Chinese with English Abstract). [[CrossRef](#)]
13. Qin, M.K.; Huang, S.H.; Liu, J.L.; Liu, Z.Y.; Guo, Q.; Jia, L.C.; Jiang, W.J. Hydrothermal alteration and its superimposed enrichment for Qianjiadian tabular-type U deposit in southwestern Songliao Basin. *Minerals* **2022**, *12*, 52. [[CrossRef](#)]
14. Bonnetti, C.; Liu, X.D.; Yan, Z.B.; Cuney, M.; Michels, R.; Malartre, F.; Mercadier, J.; Cai, J.F. Coupled U mineralisation and bacterial sulphate reduction for the genesis of the Baxingtuo sandstone-hosted U deposit, SW Songliao Basin, NE China. *Ore Geol. Rev.* **2017**, *82*, 108–129. [[CrossRef](#)]
15. Jiao, Y.Q.; Wu, L.Q.; Rong, H. Model of inner and outer reductive media within U reservoir sandstone of sandstone-type U deposits and its orecontrolling mechanism: Case studies in Daying and Qianjiadian U deposits. *Earth Sci.* **2018**, *43*, 459–474, (In Chinese with English Abstract).
16. Zhang, L.; Liu, C.Y.; Lei, K.Y. Green altered sandstone related to hydrocarbon migration from the U deposits in the northern Ordos Basin, China. *Ore Geol. Rev.* **2019**, *109*, 482–493. [[CrossRef](#)]
17. Wu, B.L.; Zhang, W.Y.; Song, Z.S.; Cun, X.N.; Sun, L.; Luo, J.J.; Li, Y.Q.; Cheng, X.H.; Sun, B. Geological and geochemical characteristics of U minerals in the sandstone-type U deposits in the north of Ordos Basin and their genetic significance. *Acta Geol. Sin.* **2016**, *90*, 3393–3407, (In Chinese with English Abstract).
18. Ding, B.; Liu, H.X.; Zhang, B.; Li, P.; Jiang, H.; Zhang, H.; Xie, X.L.; Guo, C.J. Mineralogical and isotopes evidence for origin of pyrite: Implication for formation mechanism of pyrite and its relationship with U mineralization in Mengqiguer U deposit, Yili Basin. *Miner. Depos.* **2019**, *38*, 1379–1391, (In Chinese with English Abstract).
19. Yue, L.; Jiao, Y.; Wu, L.; Rong, H.; Fayek, M.; Xie, H. Evolution and origins of pyrite in sandstone-type U deposits, northern Ordos basin, north-central China, based on micromorphological and compositional analysis. *Ore Geol. Rev.* **2020**, *118*, 103334. [[CrossRef](#)]
20. Miao, A.S.; Lu, Q.; Liu, H.F.; Xiao, P. Occurrence and formation of coffinite in ancient interlayer oxidizing zone of sandstone type U-deposit in Ordos Basin. *Geol. Sci. Technol. Inf.* **2009**, *28*, 51–58, (In Chinese with English Abstract).
21. Wang, G.; Wang, Q.; Miao, A.S.; Jiao, Y.Q.; Yi, C. Characteristic of U minerals in Nalinggou U deposit or Ordos Basin and their formation mechanism. *Acta Miner. Sin.* **2017**, *37*, 461–468, (In Chinese with English Abstract).
22. Chen, L.; Chen, Y.; Feng, X.; Li, J.G.; Guo, H.; Miao, P.; Jin, R.; Tang, C.; Zhao, H.; Wang, G.; et al. U occurrence state in the Tarangaole area of the Ordos Basin, China: Implications for enrichment and mineralization. *Ore Geol. Rev.* **2019**, *115*, 103034. [[CrossRef](#)]
23. Ding, B.; Liu, H.X.; Qiu, L.F.; Zhang, C.; Xu, D.R. Ilmenite alteration and its adsorption and catalytic reduction in U enrichment in sandstone-hosted U deposits from the northern Ordos Basin, North China. *Minerals* **2022**, *12*, 167. [[CrossRef](#)]
24. Machel, H.G.; Lonnee, L. Hydrothermal dolomite—a product of poor definition and imagination. *Sediment. Geol.* **2002**, *152*, 163–171. [[CrossRef](#)]
25. Xu, Q.; Qin, M.K.; Fan, H.H.; Gu, D.Z.; Wang, S.Y. Preliminary discussion on ore-controlling factors of Azelik sandstone type U deposits in Niger. *World Nucl. Geosci.* **2012**, *29*, 149–155, (In Chinese with English Abstract).

26. Liu, Z.Y.; Peng, S.P.; Qin, M.K.; He, Z.B.; Guo, Q.; Xu, Q. Multistage enrichment of the Sawafuqi U deposit: New Insights into Sandstone-hosted U deposits in the intramontane Basins of Tianshan, China. *Acta Geol. Sin. (Engl. Ed.)* **2017**, *6*, 2138–2152. [[CrossRef](#)]
27. Xiao, X.J.; Li, Z.Y.; Fang, X.H.; Ou, G.X.; Sun, Y.; Chen, A.P. The evidences and significances of epithermal mineralization fluid in the Dongsheng sandstone type U deposit. *Bull. Mineral. Petrol. Geochim.* **2004**, *23*, 301–304, (In Chinese with English Abstract).
28. Zhang, L.; Liu, C.-Y.; Zhao, Z.-Q.; Diao, Z.-B.; Wang, F.-F.; Song, Z.-S. Fluid evolution and mineralization of Hangjinqi sandstone-type U deposit, Ordos Basin. *Earth Sci. Front.* **2015**, *22*, 368–381, (In Chinese with English Abstract).
29. Wang, F.G.; Hou, S.R.; Zhang, L.; Men, H.; Wang, J.L. Study on the Characteristics of Water-Rock Interaction and Its Relation to Uranium Mineralization in Tamusu Uranium Deposit, Southern Bayin Gobi Basin. *Geol. Rev.* **2018**, *64*, 633–646, (In Chinese with English Abstract).
30. Zhang, C.Y.; Nie, F.J.; Jiao, Y.Q.; Deng, W.; Peng, Y.B.; Hou, S.R.; Dai, M.J.; Ye, T.F. Characterization of ore-forming fluids in the Tamusu sandstone-type uranium deposit, Bayingobi Basin, China: Constraints from trace elements, fluid inclusions and C–O–S isotopes. *Ore Geol. Rev.* **2019**, *111*, 102999. [[CrossRef](#)]
31. Zhang, Z.M.; Cai, Y.Q.; Cai, J.F.; Liu, Z.Y. Discussion on the relationship between diabase intrusion and sandstone-type uranium mineralization in the southwestern Songliao Basin: C–O isotope evidence from carbonate cement. *Geol. Rev.* **2019**, *65*, 113–114, (In Chinese with English Abstract).
32. Rong, H.; Jiao, Y.Q.; Wu, L.Q.; Zhao, X.F.; Gao, M.Q.; Liu, W.H. Effects of igneous intrusions on diagenesis and reservoir quality of sandstone in the Songliao Basin, China. *Mar. Pet. Geol.* **2021**, *127*, 104980. [[CrossRef](#)]
33. Rong, H.; Jiao, Y.Q.; Wu, L.Q.; Ji, D.M.; Li, H.L.; Zhu, Q.; Cao, M.Q.; Wang, X.M.; Li, Q.C.; Xie, H.L. Epigenetic Alteration and Its Constraints on Uranium Mineralization from the Qianjiadian Uranium Deposit, Southern Songliao Basin. *Earth Sci.* **2016**, *41*, 153–166, (In Chinese with English Abstract).
34. Jia, J.M.; Rong, H.; Jiao, Y.Q.; Wu, L.Q.; Guo, X.J.; Cao, M.Q.; Cui, Z.J.; Tao, Z.P. Occurrence of Carbonate Cements and Relationship between Carbonate Cementation and Uranium Mineralization of Qianjiadian Uranium Deposit, Songliao Basin. *Earth Sci.* **2018**, *43*, 149–161, (In Chinese with English Abstract).
35. Yang, D.G.; Wu, J.H.; Nie, F.J.; Bonnetti, C.; Xia, F.; Yan, Z.B.; Cai, J.F.; Wang, C.D.; Wang, H.T. Petrogenetic constraints of early Cenozoic mafic rocks in the southwest Songliao Basin, NE China: Implications for the genesis of sandstone-hosted Qianjiadian U deposits. *Minerals* **2020**, *10*, 1014. [[CrossRef](#)]
36. Yan, X.L. Characteristics of upper Cretaceous diabase and uranium mineralization in Qianjiadian area, Songliao Basin. *J. Northeast. Pet. Univ.* **2018**, *42*, 40–48. (In Chinese with English Abstract)
37. Liu, H.B.; Jin, G.S.; Han, J.; Zhang, J.F.; Li, J.J.; Zhang, J.; Shi, X. Element and isotope geochemical characteristics of diabase in Qianjiadian uranium deposit. *World Nucl. Geosci.* **2021**, *38*, 135–143, (In Chinese with English Abstract).
38. Deng, C.L.; He, H.Y.; Pan, Y.X.; Zhu, R.X. Chronology of the terrestrial Upper Cretaceous in the Songliao Basin, Northeast Asia. *Palaeogeogr. Palaeoclimatol. Palaeoecol.* **2013**, *385*, 44–54. [[CrossRef](#)]
39. Zhao, B.; Wang, C.; Wang, X.; Feng, Z. Late Cretaceous (Campanian) provenance change in the Songliao Basin, NE China: Evidence from detrital zircon U–Pb ages from the Yaojia and Nenjiang formations. *Palaeogeogr. Palaeoclimatol. Palaeoecol.* **2013**, *385*, 83–94. [[CrossRef](#)]
40. Dong, T.; He, S.; Wang, D.; Hou, Y. Hydrocarbon migration and accumulation in the Upper Cretaceous Qingshankou Formation, Changling Sag, Southern Songliao Basin: Insights from integrated analyses of fluid inclusion, oil source correlation and basin modelling. *J. Asian Earth Sci.* **2014**, *90*, 77–87. [[CrossRef](#)]
41. Ren, J.; Tamaki, K.; Li, S.; Zhang, J. Late Mesozoic and Cenozoic rifting and its dynamic setting in Eastern China and adjacent areas. *Tectonophysics* **2002**, *344*, 175–205. [[CrossRef](#)]
42. Li, S.Q.; Chen, F.; Siebel, W.; Wu, J.D.; Zhu, X.Y. Late Mesozoic tectonic evolution of the Songliao basin, NE China: Evidence from detrital zircon ages and Sr–Nd isotopes. *Gondwana Res.* **2012**, *22*, 943–955. [[CrossRef](#)]
43. Xia, Y.L.; Zheng, J.W.; Li, Z.Y.; Li, L.Q.; Tian, S.F. Metallogenic characteristics and metallogenic model of Qianjiadian U deposit in Songliao Basin. *Miner. Depos.* **2003**, *29*, 154–155. (In Chinese with English Abstract)
44. Zhang, M.Y.; Zheng, J.W.; Tian, S.F.; Xia, Y.L.; Liu, H.B. Research on existing state of U and U ore-formation age at Qianjiadian U deposit in Kailu depression. *Uranium Geol.* **2005**, *21*, 213–218.
45. Renaud, V.; Michel, D.; Olaf, M. Oswaldpeetersite,  $(\text{UO}_2)_2\text{CO}_3(\text{OH})_2 \cdot 4\text{H}_2\text{O}$ , a new basic uranyl carbonate mineral from the Jomac Uranium Mine, San Juan Country, Utah, U.S.A. *Can. Mineral.* **2001**, *39*, 1685–1689.
46. Samer, A.; Thuro, A.; Harald, F.; Gerhard, G.; Gert, B. Spectroscopic characterization of synthetic Becquerelite  $\text{Ca}[(\text{UO}_2)_6\text{O}_4(\text{OH})_6] \cdot 8\text{H}_2\text{O}$ , and Swartzite  $\text{CaMg}[\text{UO}_2(\text{CO}_3)_3] \cdot 12\text{H}_2\text{O}$ . *Can. Mineral.* **2004**, *42*, 953–962.
47. Bernhard, G.; Geipel, G.; Reich, T.; Brendler, V.; Amayri, S.; Nitsche, H. Uranyl(VI) carbonate complex formation: Validation of the  $\text{Ca}_2\text{UO}_2(\text{CO}_3)_3(\text{aq})$  species. *Radiochim. Acta* **2001**, *89*, 511–518. [[CrossRef](#)]
48. Lee, J.Y.; Yun, J.I. Formation of ternary  $\text{CaUO}_2(\text{CO}_3)_3^{2-}$  and  $\text{Ca}_2\text{UO}_2(\text{CO}_3)_3(\text{aq})$  complexes under neutral to weakly alkaline conditions. *Dalton Trans.* **2013**, *42*, 9862–9869. [[CrossRef](#)]
49. Endrizzi, F.; Rao, L. Chemical speciation of U(VI) in marine environments: Complexation of calcium and magnesium ions with  $[(\text{UO}_2)(\text{CO}_3)_3]^{4-}$  and the effect on the extraction of U from seawater. *Chem. Eur. J.* **2014**, *20*, 14499–14506. [[CrossRef](#)] [[PubMed](#)]
50. Brooks, S.C.; Fredrickson, J.K.; Carroll, S.L. Inhibition of bacterial U(VI) reduction by calcium. *Environ. Sci. Technol.* **2003**, *37*, 1850–1858. [[CrossRef](#)]

51. Stewart, B.D.; Mayes, M.A.; Fendorf, S. Impact of uranyl-calcium- carbonate complexes on U(VI) adsorption to synthetic and natural sediments. *Environ. Sci. Technol.* **2010**, *44*, 928–934. [[CrossRef](#)]
52. Slimane, D.D.; Vaughan, D.J.; Livens, F.R.; Burton, N.A. Atomistic Simulations of Calcium Uranyl(VI) Carbonate Adsorption on Calcite and Stepped-Calcite Surfaces. *Environ. Sci. Technol.* **2012**, *46*, 7587–7594.
53. Carroll, S.A.; Bruno, J. Mineral-solution interactions in the U(VI)-CO<sub>2</sub>-H<sub>2</sub>O system. *Radiochim. Acta* **1991**, *52–53*, 187–193. [[CrossRef](#)]
54. Geipel, G.; Reich, T.; Brendler, V.; Bernhard, G.; Nitsche, H. Laser and X-ray spectroscopic studies of U-calcite interface phenomena. *J. Nucl. Mater.* **1997**, *248*, 408–411. [[CrossRef](#)]
55. Christian, D.; Dimosthenis, S.; Thomas, K.; John, R.B.; Scott, F. Calcium-uranyl- carbonate species kinetically limit U(VI) reduction by Fe(II) and lead to U(V)-bearing ferrihydrite. *Environ. Sci. Technol.* **2020**, *54*, 6021–6030. [[CrossRef](#)]
56. Pablo, J.D.; Casas, I.; Cimenez, J. The oxidative dissolution mechanism of U dioxide.I. The effect of temperature in hydrogen carbonate medium. *Geochim. Cosmochim. Acta* **1999**, *63*, 3097–3103. [[CrossRef](#)]
57. Goldhaber, M.B.; Hemingway, B.S.; Mohagheghi, A.; Reynolds, R.L.; Northrop, H.R. Origin of coffinite in sedimentary rocks by a sequential adsorption- reduction mechanism. *Bull. Mineral.* **1987**, *110*, 131–144. [[CrossRef](#)]

**Disclaimer/Publisher’s Note:** The statements, opinions and data contained in all publications are solely those of the individual author(s) and contributor(s) and not of MDPI and/or the editor(s). MDPI and/or the editor(s) disclaim responsibility for any injury to people or property resulting from any ideas, methods, instructions or products referred to in the content.